Formic acid oxidation on Pt–Au nanoparticles: Relation between the catalyst activity and the poisoning rate

M.D. Obradović[a], J.R. Rogan[b], B.M. Babić[c], A.V. Tripković[a], A.R.S. Gautam[d], V.R. Radmilović[b,d], S.Lj. Gojković[b,*]

[a] Institute of Chemistry, Technology and Metallurgy, University of Belgrade, Njegoševa 2, 11000 Belgrade, Serbia
[b] Faculty of Technology and Metallurgy, University of Belgrade, Karnegijeva 4, 11120 Belgrade, Serbia
[c] Vinča Institute of Nuclear Sciences, University of Belgrade, P. O. Box 522, 11001 Belgrade, Serbia
[d] National Center for Electron Microscopy, Lawrence Berkeley National Laboratory, University of California, Berkeley, CA 94720, USA

ARTICLE INFO

ABSTRACT

Pt–Au nanoparticles supported on high area carbon were prepared by simultaneous reduction of Au and Pt precursors and by reduction of Pt precursor on already prepared Au nanoparticles. The first method produced a solid solution of Pt in Au containing ~5% Pt with the remaining Pt on the nanoparticles' surface. For the Pt:Au precursor ratio of 1:4 and 1:9, the surface ratio was found to be 0.70:0.30 and 0.55:0.45, respectively. By the second method with the Pt:Au precursors ratio of 1:12, the surface ratio was 0.30:0.70. The voltammetric peaks of Pt–oxide reduction and CO_{ads} oxidation demonstrated electronic modification of Pt by Au in all catalysts. With decreasing Pt:Au surface ratio the activity for HCOOH oxidation increases and surface coverage by CO_{ads} decreases. The highest activity under potentiodynamic and quasi steady-state conditions without poisoning by CO_{ads} was observed for the catalyst with the lowest Pt:Au surface ratio. Chronoamperometic test showed that its high catalytic activity is associated with a high deactivation rate. It was postulated that too strong adsorption of a reactive or non-reactive intermediate caused by electron modification of Pt by underlying Au, is responsible for the deactivation. This result stresses that high Pt dispersion, necessary for promotion of the dehydrogenation path in HCOOH oxidation, can produce too strong adsorption of intermediates causing deactivation of the catalyst.

© 2011 Elsevier B.V. All rights reserved.

1. Introduction

Polymer electrolyte membrane fuel cell (PEMFC) using formic acid as a fuel, i.e. direct formic acid fuel cell (DFAFC), has been attracting significant attention since recognition of its advantages over direct methanol fuel cell (DMFC): crossover of HCOOH through the polymer membrane is lower and the equilibrium and the onset potential of the oxidation of HCOOH is less positive compared to CH_3OH [1,2].

Pt is not suitable electrocatalyst for HCOOH oxidation because it is prone to the poisoning by CO_{ads} formed in dehydration path. This makes most of the Pt surface unavailable for HCOOH oxidation through dehydrogenation path [3]. The initial activity of Pd is much higher comparing to Pt, but deactivation of Pd over time is significant [4] and Pd is not stable in acid media [5]. A solution of the problem of HCOOH oxidation catalysis is to use Pt-based bimetal catalysts. Although bifunctional mechanism and electronic effect can influence oxidative removal of CO_{ads} from the Pt sites, the

better approach is to prevent CO_{ads} formation by employing ensemble effect, i.e. to increase selectivity of Pt toward dehydrogenation path. This is based on the recent study of HCOOH oxidation on Pt(1 1 1) modified by cyanide ions performed by Cuesta et al. [6] in which they established that at least three contiguous Pt sites are necessary for dehydration of HCOOH, while at most two Pt sites are required for dehydrogenation of HCOOH.

After early work of Rach and Heitbaum [7], many articles published in the last several years confirmed that HCOOH on Pt–Au surfaces exhibits high current densities at low potentials with much less CO_{ads} on the surface than single Pt catalyst [8–16]. Although some other metals like Bi [17] and Pb [18] showed similar promotion of the dehydrogenation path on Pt, Pt–Au catalysts are more promising for practical application in DFAFC because of great chemical stability of Au.

General feature of the HCOOH oxidation catalysis on Pt–Au bimetal surfaces is that decreasing Pt content in the catalyst favors dehydrogenation path. In our previous work [13] we used bulk Pt electrode modified by submonolayers of Au and Au electrodes modified by submonolayers of Pt to demonstrate that increased selectivity toward dehydrogenation path in HCOOH oxidation is mainly caused by an ensemble effect. The electronic modification

of Pt by Au, which might increase interaction of HCOOH molecule with Pt, probably contributes to rather low onset potential of the reaction [8,10]. Among several types of Pt–Au nanocatalysts, the best performance (high current density without CO_{ads} poisoning) was exhibited by Pt-decorated Au nanoparticles with Pt:Au ratio of 1:8 [10] and by Pt decorated nanoporous Au, previously annealed to enable surface alloying and good dispersion of Pt and Au [12].

This paper reports the synthesis of Pt–Au nanoparticles supported on high area carbon by simultaneous reduction of Au and Pt precursors and by reduction of Pt precursor on already prepared Au nanoparticles; and compares their activity for HCOOH oxidation. For the first time the reaction orders with respect to HCOOH and H^+ ions were determined for the Pt surface unpoisoned by CO_{ads}. A problem of rapid deactivation of Pt–Au nanocatalyst with high initial activity is observed and discussed.

2. Experimental

2.1. Preparation of the catalysts

Au and bimetallic Pt–Au nanoparticles supported on high area carbon were prepared by microwave-assisted polyol method [19,20]. The advantage of microwave over conventional heating during nanoparticles synthesis is uniform heating of the substrate by the electromagnetic waves leading to a more homogeneous nucleation and shorter aggregation time. Another type of Pt–Au nanoparticles was prepared by decoration of Au nanoparticles with Pt by using ascorbic acid ($C_6H_8O_6$) as the reducing agent [8,21]. It was found that ascorbic acid as a weak reducing agent with a slower reduction rate in respect to $NaBH_4$ or NH_2OH, forms nanoparticles with better monodispersity and morphology [21].

In the first synthesis carbon black (Vulcan® XC-72R, produced by Cabot Corp., BET specific surface area $246\,m^2\,g^{-1}$) was added in ethylene glycol and ultrasonicated over 1 h. Than $HAuCl_4$ (10% solution, Alfa Aesar), or a mixture of H_2PtCl_6 (10% solution, Alfa Aesar) and $HAuCl_4$ was added in the suspension of carbon black in ethylene glycol. pH of the suspension was adjusted to ~8. After heating for 60 s in the microwave oven (Samsung, 2450 MHz, 600 W), the suspension was vacuum-filtered and the powder was washed with $0.02\,M\,NH_4OH$, as it was shown that chloride anions can be eliminated from the samples by washing with ammonia solution of low concentration [22]. All the prepared samples were dried in Ar atmosphere at $80\,°C$ over 8 h. The Pt–Au/C catalysts of two different compositions were prepared by mixing precursors in Pt:Au atomic ratio of 1:4 and 1:9. The corresponding catalysts are labeled according to the preparation method (polyol – P) and overall ratio of Pt and Au atoms as P-1:4 and P-1:9.

Prepared Au/C was modified with Pt in accord to a typical preparation of core–shell Au–Pt colloid [4,8]. A suspension containing $1.0\,mg\,cm^{-3}$ Au/C was mixed with $0.20\,M\,H_2PtCl_6$ solution in the amount to get 1:1 ratio of surface Au atoms and Pt(IV) ions. The surface of Au nanoparticles was estimated from the average Au grain size determined in XRD measurements. This Pt:Au ratio correspond to the overall composition ratio of 1:12. Next, 0.1 M solution of ascorbic acid was added to the suspension. The molar ratio of ascorbic acid and Pt ions was 4:1. After stirring for 20 h, the suspension was precipitated, washed, and dried in Ar atmosphere at $80\,°C$ over 8 h. The prepared electrocatalyst is also labeled according to the preparation method (ascorbic acid, AA) and overall Pt:Au atomic ratio, as AA-1:12.

For a comparison of voltammetric features and electrocatalytic activity, a sample of Pt nanoparticles supported on XC-72R carbon (Pt/C), manufactured by E-Tek, was used. According to Esparbé et al. [23], this catalyst consists of Pt nanoparticles with an average diameter of 2.5 nm and electrochemically active surface area of $73\,m^2\,g\,Pt^{-1}$.

2.2. Thermogravimetric analysis

Metal loading of the Au and Pt–Au/C samples was determined by thermogravimetric analysis (TGA) [24] using a SDT Q600 TGA/DSC instrument (TA Instruments). Several milligrams of the sample were heated to $800\,°C$ at the heating rate of $20\,°C\,min^{-1}$ in the air atmosphere (flow rate $100\,cm^3\,min^{-1}$). Upon measuring of metal mass in the residual ash, metal loading was calculated to be between 12 and 19 mass%, and these data were used for calculation of specific surface area of the catalysts.

2.3. XRD and TEM characterization

The synthesized samples were examined by X-ray diffraction (XRD) in order to determine phase composition and to estimate particle size. The measurements were carried out with a SIEMENS D500 diffractometer operated with a CuKα source at 35 kV and 20 mA in the 2θ range from 10° to 100° with $0.02°\,2\theta\,s^{-1}$. High resolution transmission electron microscopy (HRTEM) was used to characterize morphology and size of the nanoparticles and their distribution on the carbon support. The measurements were performed at the National Center for Electron Microscopy using the TEAM I TEM/STEM double-aberration-corrected electron microscope at 80 kV equipped with the Gatan $2k \times 2k$ CCD cameras.

2.4. Electrochemical characterization

For electrochemical characterization, the Pt/C, Au/C, and Pt–Au/C powders were applied on a glassy carbon (GC) substrate in the form of a thin-film [25]. The GC electrode (Tacussel rotating disk electrode, 5 mm in diameter) was polished with 1, 0.3, 0.05 μm Al_2O_3 slurry and washed ultrasonically with high purity water (Millipore, $18\,M\,\Omega\,cm$ resistivity) before use. The catalyst inks were made by mixing of 2.0 mg of the powder with $1\,cm^3$ of high purity water and 50 μL of the Nafion® solution (5 wt.%, 1100 E.W., Aldrich). After 1 h of agitation in an ultrasonic bath, 10 μL of the suspension was placed onto the GC electrode and left to dry overnight. This procedure of film preparation gave 0.10 mg of powder per cm^2 of the GC surface.

A three-compartment electrochemical glass cell was used with a Pt wire as the counter electrode and a saturated calomel electrode as the reference electrode. All the potentials reported in the paper are expressed on the scale of the reversible hydrogen electrode (RHE). The cyclic voltammetry was carried out in $0.05–1.0\,M\,H_2SO_4$ (Merck) prepared with high purity water. The electrolytes were deaerated by the N_2 bubbling. Upon immersion into the electrolyte, a thin-film electrode was pre-conditioned by the potential cycling between 0.05 and 1.46 V at $0.1\,V\,s^{-1}$. After ten cycles the scan rate was reduced to $0.05\,V\,s^{-1}$ and the second cycle was recorded and used for the surface characterization.

The electrochemical active area of Au was determined from the reduction of the monolayer of gold oxide formed under the potential cycling with the anodic limit just before the onset of oxygen evolution, i.e. at the Burshtein's minimum [26]. The charge of the reduction of monolayer gold oxide was taken to be $400\,\mu C\,cm^{-2}$ [12,27].

The electrochemically active area of Pt in Pt/C catalyst was calculated from the hydrogen desorption charge corrected for the double-layer charging assuming $210\,\mu C\,cm^{-2}$ for monolayer hydrogen adsorption. However, for Pt–Au surfaces, especially those with low Pt content, this method was found to be unreliable because hydrogen adsorption/desorption features were barely seen or even absent, although the peak for Pt–oxide reduction and a

high activity for HCOOH oxidation undoubtedly showed that Pt was present on the surface. The anodic stripping of adsorbed CO was also found unsuitable for the Pt surface area determination. On Pt/C catalyst the CO_{ads} stripping charge corresponded to a monolayer on Pt surface area calculated from hydrogen desorption charge, but a problem was encountered on bimetallic Pt–Au surfaces. On the surface of Au nanoparticles, as opposed to bulk Au surface, CO adsorption cannot be neglected. Therefore, we determined Pt surface area on Pt–Au surfaces from the Pt–oxide reduction peak using a charge of $440\,\mu C\,cm^{-2}$ for a Pt–oxide monolayer [8]. This value was confirmed in our experiments by comparing charges for hydrogen desorption and Pt–oxide reduction on Pt nanoparticles in Pt/C catalyst. Besides, in the previous study of Pt submonolayers on bulk Au [13], where hydrogen adsorption/desorption peaks were also ill-defined, Pt surface area was determined by the same method. These experiments showed that the sum of the surface areas of Pt and Au, both determined form the oxide reduction charges, was equal to the surface area of Au before modification by Pt, thus verifying the reliability of the method. Recently Irissou et al. [28] investigated surfaces of the thin films of Pt–Au alloys and concluded that the Pt and Au surface areas determined by X-ray photoelectron spectroscopy and electrochemically by integrating metal oxide reduction peaks yielded similar values ($\pm4\%$).

Prior to CO stripping voltammetry pure CO was bubbled through the electrolyte for 30 min while keeping the electrode potential at 0.10 V [8]. After purging the electrolyte by N_2 for 30 min to eliminate dissolved CO, adsorbed CO was oxidized in an anodic scan at $20\,mV\,s^{-1}$. Two subsequent voltammograms were also recorded to verify the completeness of the CO oxidation.

Electrochemical oxidation of HCOOH was investigated in deaerated supporting electrolyte containing from 0.05 to 1.0 M HCOOH (Merck). In the positive going scan, the potential was held at 0.10 V and HCOOH was added into the electrolyte. After 2 min the scan was continued at the rate of $1\,mV\,s^{-1}$ (quasi steady-state measurements) or at $50\,mV\,s^{-1}$ (potentiodynamic measurements).

The experiments were conducted at constant temperature of $298\pm0.5\,K$. A Pine RDE4 potentiostat and Philips PM 8143 X–Y recorder were employed.

3. Results and discussion

3.1. XRD characterization of the nanocatalysts

XRD patterns of the prepared Au/C and bimetallic P-1:4 and P-1:9 catalysts are presented in Fig. 1 along with the reference spectrum of Au and Pt taken from JCPD cards. The peak positions of P-1:4 and P-1:9 catalysts are almost the same, but slightly shifted toward higher angles with respect to those of Au/C. From the Au(2 2 0) reflections of P-1:4 (64.99°), P-1:9 (65.01°), Au/C (64.85°), and Pt/C (67.70°, not shown), and assuming Vegard's law, it was calculated that Pt contents in P-1:4 and P-1:9 catalysts are 5.3 at.% and 5.9 at%, respectively. The alloying degree of Pt in the catalysts, calculated according to equation [29]:

$$Pt_{alloy} = \frac{x_{Pt}}{(1-x_{Pt})\cdot(n_{Pt}/n_{Au})_{nominal}}$$

was found to be 22% for P-1:4 and 55% for P-1:9. This means that Pt is distributed between Au–Pt solid solution and an amorphous phase undetectable by XRD that is probably pure Pt. Barely visible broadening of (1 1 1) and (2 0 0) peaks of Au in P-1:4 and P-1:9 samples toward higher angles i.e. toward the peak of pure Pt concurs this assumption. As expected, the AA-1:12 sample showed the same XRD pattern as Au/C (not shown) due to very low Pt content.
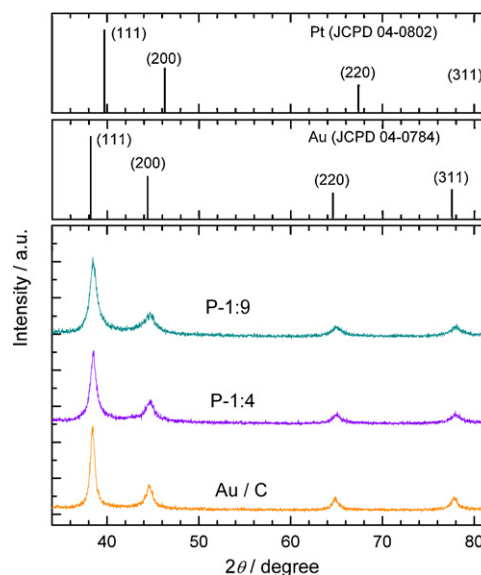

Fig. 1. XRD patterns of P-1:4, P-1:9, and Au/C samples. The 2θ positions for bulk Au and Pt are shown on the plot for the reference.

3.2. TEM imaging of the nanocatalysts

The Au/C and P-1:9 samples were characterized using TEM. The image of Au/C (Fig. 2a) shows Au nanoparticles of approximately spherical shape those are well-dispersed on carbon support. Fig. 2b presents image of P-1:9 catalyst with many nanoparticles of irregular shape. Although XRD analysis indicated two-phase structure of the catalyst (solid solution of Pt in Au and pure amorphous Pt) and cyclic voltammetry showed that about 55% of the catalyst surface is Pt (see below), this cannot be confirmed by TEM because of the small difference between Au and Pt lattice constant.

3.3. Cyclic voltammetry of the nanocatalysts

Cyclic voltammograms of all the examined nanocatalysts are presented in Fig. 3. The current densities are given per total electrochemically active surface area of Pt and Au for the single metal catalysts and per total Pt + Au surface area for the bimetal catalysts. The voltammogram for Pt/C reveals well-established characteristics of a clean polycrystalline Pt surface. Hydrogen adsorption/desorption processes take place at the potentials between 0.03 and 0.30 V, followed by a so-called Pt double layer region, which is broaden due to the double layer capacitance of high area carbon. At the potentials over 0.8 V Pt–oxide is formed and reduced in the negative-going sweep yielding the peak at ~0.72 V. The voltammograms of P-1:4 and P-1:9 catalysts show the same features as Pt/C, but suppressed and with the significant negative shift in the peak potential of Pt–oxide reduction. This negative shift is an indication of the electronic modification of Pt atoms by the neighboring Au atoms. The presence of Au on the surface is identified by the peak of the Au–oxide reduction at ~1.15 V, which corresponds to the voltammogram of Au/C given in the inset of Fig. 3.

The voltammograms of Au/C and AA-1:12, given in the inset in Fig. 3, show the current of Au oxidation and the Au–oxide reduction peak. In the case of AA-1:12 the charge for the Au–oxide reduction is lower, indicating partial coverage of Au by Pt. The presence of Pt is confirmed by the peak of Pt–oxide reduction at ~0.62 V, although hydrogen adsorption/desorption features are not resolved. Ill-developed or even absent hydrogen adsorption/desorption features on monolayer Pt deposited on Au has been reported [15,30].

Table 1
Particle size and surface area determined by XRD and electrochemically active surface areas of Pt and Au (per total mass of metals) determined by cyclic voltammetry for Pt/C, Au/C, and Pt–Au/C catalysts of different Pt:Au ratio of the precursors.

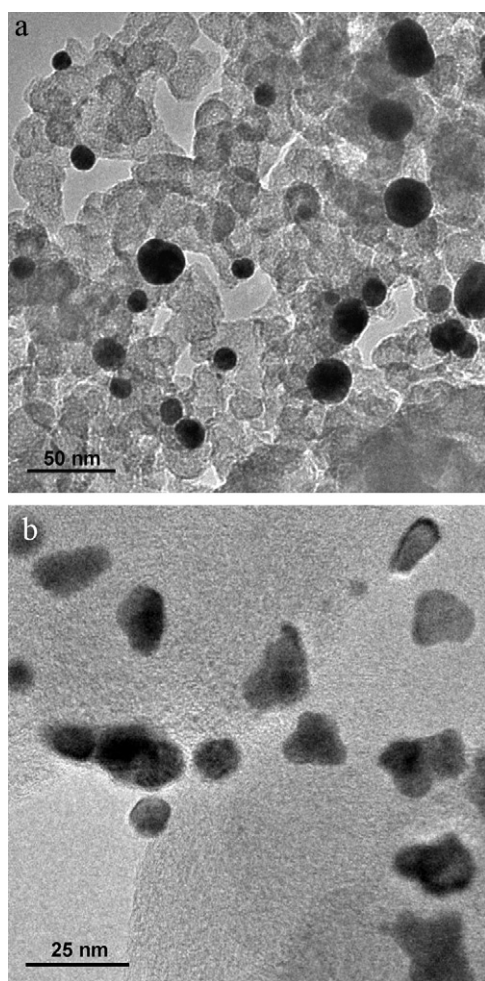| Sample	Pt/C	P-1-4	P-1-9	AA-1-12	Au/C
Pt: Au precursor ratio	–	1:4	1:9	1:12	–
d(XRD)/nm	2.5[a]	~8.1	~11.2	18.3	18.3
S(XRD)/m^2 g^{-1}	112	37	27	16	17
S_{Pt}/m^2 g^{-1}	68	17	12	4.1	–
S_{Au}/m^2 g^{-1}	–	8	10	8.1	13
S_{Pt+Au}/m^2 g^{-1}	–	25	22	12	13
Pt:Au surface ratio		0.7:0.3	0.55:0.45	0.3:0.7	

[a] Taken from Ref. [23].

Fig. 2. TEM images of (a) Au/C and (b) P-1:9 nanocatalysts.

The electrochemically active surface area of Pt and Au for all the samples, determined from the cyclic voltammograms by integrating the Pt–oxide and Au–oxide reduction peaks, is given in Table 1 along with the particle size determined in XRD measurements and the resulting surface area. The particle sizes for the P-1:4 and P-1:9 samples are only approximate, because Scherrer equation is strictly applicable to the single phase particles [8]. As one can see, the total electrochemically active surface area of Pt and Au is lower than the surface area calculated from the XRD, which could be a consequence of incomplete wetting of the catalyst, imperfect electric contact between catalyst particles and partial blocking of the catalyst particles due to the adsorption on the high area carbon support [31].
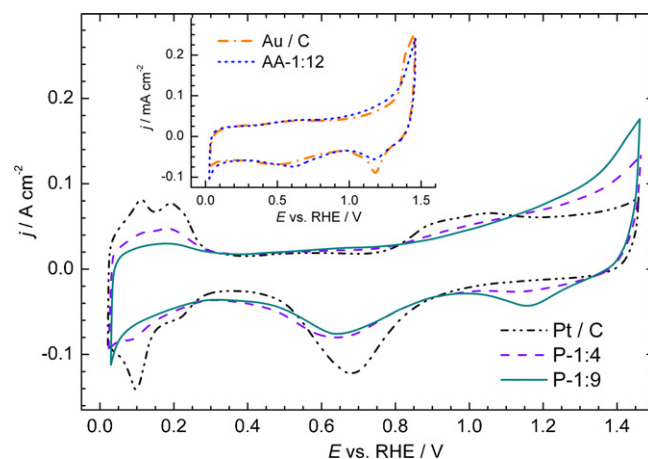
Fig. 3. Cyclic voltammograms of Pt/C, P-1:4 and P-1:9 and in insert Au/C and AA-1:12, recorded in 0.5 M H$_2$SO$_4$ at the sweep rate of 50 mV s^{-1}. The current densities were calculated per electrochemically active surface area of Pt and Au for single metal catalysts and per total Pt + Au surface area for bimetal catalysts.

3.4. Evaluation of the structure of the catalysts

The structure of bimetallic nanocatalysts can be recognized by the contrasting results of XRD and cyclic voltammetry measurements. Here one should be aware that XRD is essentially a bulk method for nanoparticles because of penetration depth of X-ray, while cyclic voltammetry reflects only the surface characteristics.

XRD measurements indicated that bulk composition of both P-1:4 and P-1:9 nanoparticles is solid solution of Pt in Au with ~5% of Pt. As alloying degree of Pt is 22% for P-1:4 catalyst and 55% for P-1:9 catalyst, the remaining Pt must be in a separate phase. Results in Table 1 show that the electrochemically active surface area of Pt in those catalysts is larger than that of Au although the amount of Au is four or nine times larger. Two different catalyst structures could rationalize these findings. The first is that unalloyed Pt is in the form of nanoparticles that are deposited directly on carbon support. The diameter of those Pt nanoparticles should be very small because XRD did not show peaks of pure Pt. However, cyclic voltammetry demonstrated negative shift of Pt–oxide reduction that is attributed to electronic modification of Pt by Au, for which an intimate contact of Pt and Au is necessary. Therefore, existence of separate Pt–Au alloy and Pt nanoparticles does not look probable. The second possibility is that unalloyed Pt is concentrated on the surface of the Pt–Au alloy nanoparticles. Taking into account the total amount of Pt and Au, degree of Pt alloying and nanoparticles size estimated from XRD, it can be calculated that the ratio of unalloyed Pt atoms and atoms on the nanoparticle surface is 1.1 for P-1:4 catalyst and 0.45 for P-1:9 catalyst. Based on this calculation and Pt:Au surface ratio estimated by cyclic voltammetry, structure of P-1:4 P-1:9 catalysts can be described as Pt–Au alloy decorated by near-monolayer Pt islands.
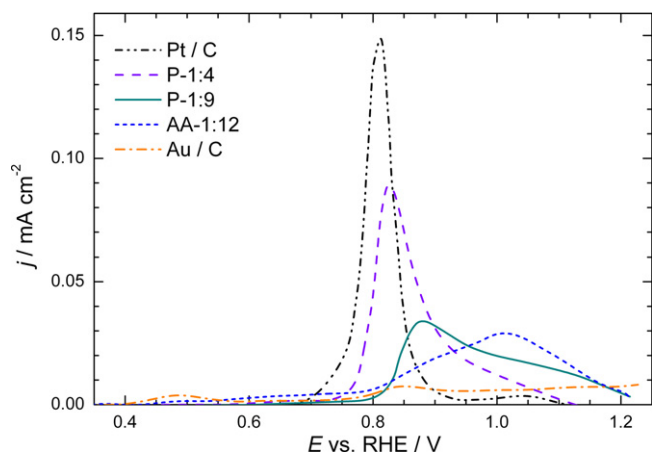
Fig. 4. CO$_{ads}$ stripping voltammograms on Pt/C, P-1:4, P-1:9, AA-1:12, and Au/C, recorded in 0.5 M H$_2$SO$_4$ at the sweep rate of 20 mV s^{-1}. The current densities were calculated per electrochemically active surface area of Pt and Au for single metal catalysts and per total Pt + Au surface area for bimetal catalysts.
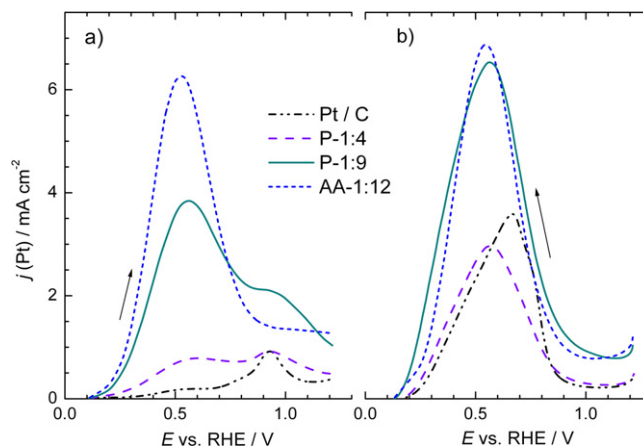

Fig. 5. Potentiodynamic polarization curves for the oxidation of HCOOH on Pt/C, P-1:4, P-1:9, AA-1:12, and Au/C recorded in (a) positive going scan and (b) negative going scan at the scan rate of 50 mV s^{-1}. Electrolyte is 0.5 M H$_2$SO$_4$ + 0.5 M HCOOH.

The data for AA-1:12 show that, despite the 1:1 molar ratio of Pt precursor and the surface Au atoms in Au/C powder, a complete Pt shell was not produced. As total surface area of the AA-1:12 catalyst is approximately the same as the surface area of Au nanoparticles in Au/C on which Pt was deposited (Table 1), it seems that Pt is in the form of near-monolayer islands rather than in the form of small nanoparticles adsorbed on larger Au nanoparticles.

One more effect could possibly influence the structure of the surface of all three bimetallic catalysts. Although Pt and Au have high melting points, Ge et al. [12] demonstrated that thermal annealing at temperatures as low as 100 °C induces surface alloying of Pt with Au substrate. Since our samples were dried at 80 °C for 8 h, it is quite possible that certain degree of a surface alloy is produced.

3.5. CO$_{ads}$ stripping voltammetry

CO$_{ads}$ stripping voltammetry was performed to further probe the surface structure and electronic modification of Pt by Au. As shown in Fig. 4, CO$_{ads}$ oxidation on Pt/C catalyst starts at ~0.69 V and exhibits a sharp peak with the maximum at 0.81 V, while the oxidation of CO$_{ads}$ on bimetallic nanoparticles is delayed with respect to Pt/C and the peak potential is as more positive as the Pt:Au surface ratio decreases. As cyclic voltammograms in Fig. 3 shows, on Pt–Au bimetallic surfaces Pt–oxide formation commences at more positive potentials than on Pt/C, which can explain hindered CO$_{ads}$ oxidation. Also, stronger adsorption of CO and OH species on Pt in contact with Au has already been reported for Pt modified Au substrate [28,32] and ascribed to the ligand effect arising from the heterometallic bonding between Pt and Au and the tensile strain experienced by Pt deposited on Au because of different lattice constants. Both effects cause the increase in d-band energy of Pt and consequent stronger bond with the adsorbates [33,34]. With decreasing Pt fraction on the surface more Pt atoms are in direct contact with Au and the electronic modification is more prominent thus causing the potential of CO$_{ads}$ oxidation shifts to more positive values.

Although CO$_{ads}$ oxidation peak on AA-1:12 catalyst is the most positive compared to the others, the onset potential on this catalysts is rather low, which can be attributed to the adsorption of CO on uncovered Au surface. As the CO$_{ads}$ stripping voltammogram for Au/C shows, CO is adsorbed on Au nanoparticles and oxidized in two potential regions, between 0.4 and 0.6 V and over 0.75 V, but the charge under the peaks corresponds to an amount of CO$_{ads}$ much lower than monolayer. The similar result was reported by

Park et al. [8]. It should be noted that, regarding CO adsorption, bulk and nano-sized Au behave differently, since CO adsorption on bulk Au was found to be negligible [13].

The sharpness and the symmetry of the CO$_{ads}$ stripping peak generally reflects the uniformity of Pt surface [35]. As the fraction of Pt on the nanoparticle surface decreases, the stripping peak becomes broader and asymmetrical, indicating finer distribution of Pt atoms on the nanoparticle surfaces. It can also be concluded that there is no Pt nanoparticles attached directly to carbon, since in this case a pre-peak at ~0.8 V characteristic for unmodified Pt would appear.

3.6. Formic acid oxidation: potentiodynamic and quasi steady-state polarization measurements

Potentiodynamic polarization curves of the HCOOH oxidation recorded on Pt/C and three bimetallic Pt–Au nanocatalysts are presented in Fig. 5. The currents recorded on Au/C electrode were much lower, so this curve is omitted from the diagram. As our investigations were focused on the activity of Pt sites on the Pt–Au surfaces, the current densities for bimetallic surfaces were calculated per Pt surface. Potentiodynamic profile of Pt/C shows well-established feature of the formic acid oxidation on Pt [3,36,37]. In the forward sweep (Fig. 5a) the current densities reach a plateau at about 0.55 V followed by the ascending current starting at 0.7 V and a high maximum at 0.93 V. The current densities below 0.7 V are attributed to HCOOH oxidation through the dehydrogenation path on the surface partially covered by CO$_{ads}$ formed by HCOOH dehydration. As formation of oxygen containing species on Pt starts, CO$_{ads}$ is oxidized, more Pt sites are being released and the HCOOH oxidation current increases until Pt–oxide, inactive for HCOOH oxidation, is formed. This results in the current peak.

As Fig. 5a shows, at bimetallic Pt–Au nanocatalysts the oxidation of HCOOH commences at lower potentials than on single Pt nanoparticles and the shape of the polarization curves are changed. As Pt:Au surface ratio decreases, the plateau corresponding to HCOOH dehydrogenation increases and transforms to peak. Also the peak corresponding to the reaction on the Pt sites released after CO$_{ads}$ oxidation decreases and even vanishes on the curve for AA-1:12 catalyst. These results show that the CO$_{ads}$ coverage of Pt sites on bimetallic surfaces is reduced in comparison to single Pt surface with CO$_{ads}$ being completely absent on the catalyst with the lowest Pt:Au surface ratio. The anodic stripping of CO$_{ads}$ (Fig. 4) showed that Pt on bimetallic Pt–Au surfaces binds CO$_{ads}$ stronger than pure Pt. This implies that lower coverage by CO$_{ads}$
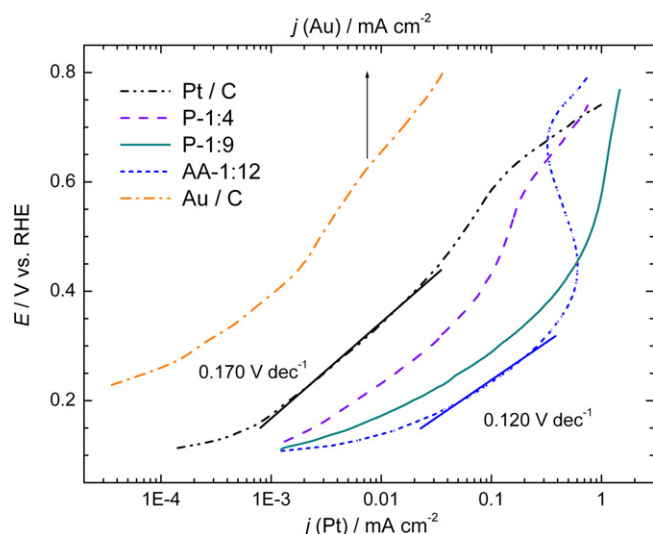
Fig. 6. Quasi steady-state polarization curves for the oxidation of HCOOH in 0.5 M H_2SO_4 + 0.5 M HCOOH electrolyte recorded on Au/C, Pt/C, P-1:4, P-1:9, and AA-1:12 at the scan rate of 1 mV s^{-1}.

during HCOOH oxidation on bimetallic surfaces is caused by suppression of the dehydration path in HCOOH oxidation mechanism rather than by facilitated CO_{ads} oxidation.

In a recent work of Grozovski et al. [38] the polarization curves of HCOOH oxidation on different Pt nanoparticles were determined by the pulsed voltammetry transients. In that way, they measured the activity of the electrode through the dehydrogenation path in the absence of poison. The maximum current densities for the Pt nanoparticles with preferential (1 0 0), (1 0 0–1 1 1) and (1 1 1) orientation were 7, 5.5 and 3 mA cm^{-2}, respectively. The maximum currents observed on the potentiodynamic polarization curves for P-1:9 and AA-1:12 catalysts were 4 and 6.5 mA cm^{-2}, respectively, which confirms that there is no significant poisoning of these two catalysts.

The backward sweeps of HCOOH oxidation are presented in Fig. 5b. On the Pt/C catalyst the current density rises at ~1 V, which is the potential where Pt–oxide reduction commences (Fig. 3). At 0.67 V the current density starts to decrease again because CO_{ads}, which is inevitably formed at a single Pt catalyst, cannot be oxidized any more (Fig. 4). Lower current densities on the ascending part of the curve for P-1:4 can be explained by the stronger adsorption of CO that makes more difficult to oxidize CO_{ads} and release Pt sites for further reaction. For the P-1:9 and AA-1:12 catalysts on which dehydration path is minor, the current densities in the backward sweep are high and reflect intrinsic activity of clean Pt surface toward HCOOH oxidation. If the forward and backward potentiodynamic curves for AA-1:12 are compared, one can see that they are almost the same, which confirms that poisoning CO_{ads} is not formed, i.e. dehydration path is completely suppressed.

Kinetics of formic acid oxidation under the quasi steady-state conditions is presented in Fig. 6 in the form of Tafel plots. The logarithmic scale of the current axis enables presenting HCOOH oxidation currents on Au/C that are for more than an order of magnitude lower than on Pt/C. The order of activity for Pt single metal and bimetal catalysts is the same as under the potentiodynamic conditions. Nanoparticles with lower Pt surface area, i.e. better distribution of Pt on Au surface are more active than single Pt nanoparticles. The most active AA-1:12 exhibits up to forty time larger current densities than Pt/C (at 0.25 V). Although linear Tafel regions are not well defined, it can be estimated that the Tafel slope decreases with the decrease in Pt:Au ratio, which was found to be related to reducing CO_{ads} coverage [37,39].
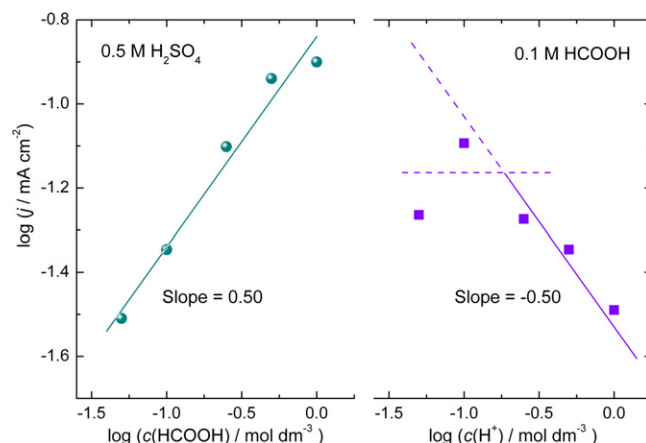

Fig. 7. Current densities of the HCOOH oxidation at 0.3 V recorded under the quasi steady-state conditions on P-1:9 as function (a) HCOOH concentration and (b) pH.

3.7. Formic acid oxidation: reaction order determination

Reaction orders with respect to HCOOH and H$^+$ ions were determined on P-1:9 catalyst. Two sets of quasi steady-state polarization curves were recorded. Firstly, HCOOH concentration was varied between 0.05 M and 1 M in 0.5 M H_2SO_4 and the current densities at the constant potential of 0.3 V are plotted as a function of HCOOH concentration. As Fig. 7a presents, a straight line with a slope of 0.5 is obtained, which is equal to the reaction order with respect to HCOOH. Then the concentration of H_2SO_4 was varied while keeping HCOOH concentration of 0.5 M. The dependence of the current densities on the H$^+$ ion concentration plotted in Fig. 7b shows that the reaction order with respect to H$^+$ ions is −0.5 at the concentrations over ~0.2 M. At lower concentrations, the reaction rate seems to be independent of the H$^+$ ion concentration.

The reaction orders for HCOOH oxidation were previously determined on Pt/C [37] and mesoporous Pt [40], on which the reaction proceeds through dehydrogenation path on the surface partially blocked by CO_{ads} produced in dehydration path occurring in parallel. It was found that HCOOH oxidation follows a half order reaction kinetics with respect to HCOOH up to 0.5 M HCOOH, but in more concentrated electrolytes the reaction rate became independent of the HCOOH concentration [37,40]. The dependence of the reaction rate on the H$^+$ ion concentration [37] exhibited the reaction order of −0.8 in the range of 0.1–1 M $HClO_4$ solution and zero reaction order in more diluted acid.

According to the potentiodynamic polarization curves in Fig. 5, the HCOOH oxidation on P-1:9 occurs on the Pt surface with very low coverage by CO_{ads}, but the reaction order values are basically the same as those on Pt with high CO_{ads} coverage. Half-order kinetics with respect to HCOOH indicates relatively high Pt coverage by the reactive intermediate in dehydrogenation path on both poisoned and unpoisoned surface.

3.8. Formic acid oxidation: chronoamperometric measurements

The chronoamperometric test of Pt/C and Pt–Au/C nanocatalysts toward HCOOH oxidation was carried out at 0.30 V for 20 min and the results are presented in Fig. 8. The activity of all the catalysts gradually decreased over time with the best long-term activity exhibited by P-1-9. However, the behavior of AA-1:12 catalyst, which was found to be the most active catalyst under the potentiodynamic and quasi steady-state conditions, deserves attention.

At the very beginning of the transient the AA-1:12 catalyst is the most active one, but its activity steeply decreases and after ~7 min drops to zero. The first assumption was that instability of Pt islands
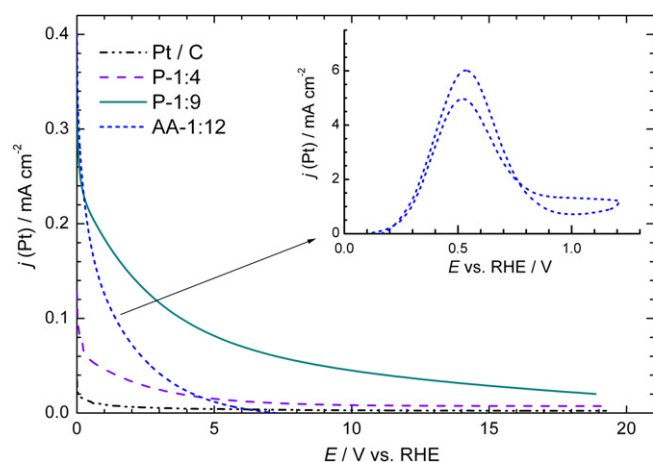
Fig. 8. Chronoamperometric measurement of HCOOH oxidation rate on Pt/C, P-1:4, P-1:9, and AA-1:12 catalysts at 0.3 V in 0.5 M H_2SO_4 + 0.5 M HCOOH electrolyte. Inset: potentiodynamic polarization curve recorded on AA-1:12 after its complete deactivation. Scan rate 50 mV s^{-1}.

on the Au surface is responsible for the activity loss. To test this hypothesis, the potentiodynamic curve was recorded for this catalyst after it had been deactivated. As the inset in Fig. 8 shows, a bell-shaped profile characteristic for dehydrogenation path of HCOOH with no poisoning by CO_{ads} was recovered, meaning that composition of the catalyst was not changed. Another possible reason for the deactivation of the AA-1:12 catalyst might be a blockage of the surface by the CO_2 bubbles, since CO_2 evolution on this catalyst is more severe than on the other two due to its high activity. However, starting the rotation of the electrode after the current had dropped to zero did not produce any increase of the current. This also proved that the near-electrode layer was not depleted of HCOOH, although this effect was not expected because of high HCOOH concentration in the electrolyte. Besides the mechanical blocking of the surface, CO_2 can cause the deactivation of Pt sites if it is reduced by the adsorbed hydrogen atoms since product of this reaction is CO_{ads} [41,42]. According to the voltammograms in Fig. 3, at the potential of 0.3 V at which chronoamperometric experiment was performed, hydrogen atoms are already desorbed from Pt/C, P-1:4 and P-1:9 bimetal catalyst. However, because of characterless voltammogram of AA-1:12 in the hydrogen adsorption/desorption region, it is difficult to estimate whether adsorbed hydrogen is present on the surface, thus deactivation by CO_{ads} produced by the CO_2 reduction cannot be excluded.

The influence of the processes on Au surface in HCOOH solution should also be considered, because of a high Au:Pt surface ratio in AA-1:12 catalyst. The activity of Au for HCOOH oxidation is low, as shown in Fig. 6. According to Koper and co-workers [43], CO_{ads} was not detected and the reason for this is slow oxidation of $HCOO_{ads}$ intermediate. Thus, surface diffusion of CO_{ads} from Au to Pt sites does not seem as a probable cause of deactivation of AA-1:12.

Surface of an electrocatalyst can be poisoned by non-reactive intermediate formed in a parallel path, but too strong adsorption of the reactive intermediate or even reaction product could also decrease number of active sites available for the reaction. Mathematical modeling of HCOOH oxidation current decay on polycrystalline Pt performed by Wieckowski and co-workers [44] also indicated that an adsorbate other than CO_{ads} has to be present on the surface in order to account for the total current decay. They speculated that intermediate forms of HCOOH, e.g. $HCOO_{ads}$, can be responsible for the current decay. Osawa and co-workers [45,46] showed that in the dual path mechanism $HCOO_{ads}$ is the reactive intermediate, although Behm and co-workers [47] consider it as non-reactive intermediate in a triple-path mechanism with direct

oxidation of HCOOH to CO_2 via still undetectable active intermediate.

The reason why AA-1:12 is more susceptible to the poisoning than the other two Pt–Au nanocatalyst could be in the strongest electronic modification of Pt by neighboring Au atoms because in this catalyst the Pt:Au surface ratio is the lowest and consequently the number of Pt atoms in close contact with Au is the highest. It was theoretically predicted [33,34] that electronic modification of Pt by Au leads to stronger bonding of any adsorbate and our experiments indicated that OH_{ads} and CO_{ads} removal from Pt sites is the slowest on AA-1:12 catalyst.

4. Conclusions

Two methods of synthesis were applied to prepare Pt–Au nanocatalysts supported on high area carbon. The first was simultaneous reduction of Au and Pt precursors in the atomic ratio of 1:4 and 1:9. As the Pt alloying was incomplete, nanoparticles were composed of solid solution of Pt in Au with ∼5% Pt in both cases, while the remaining Pt was on the nanoparticles' surfaces. Surface ratio of Pt:Au was found to be 0.70:0.30 and 0.55:0.45 for the precursors ratio 1:4 and 1:9, respectively. The second method of synthesis was reduction of Pt precursor on already prepared Au nanoparticles. With the Pt:Au precursors ratio of 1:12, which corresponded to complete monolayer Pt shell, the achieved surface ratio of Pt:Au was 0.30:0.70.

The voltammetric peaks of Pt–oxide reduction and CO_{ads} oxidation demonstrated electronic modification of Pt by Au, a degree of which increased with the decreasing Pt:Au surface ratio.

The activity for HCOOH oxidation, determined under potentiodynamic and quasi steady-state conditions, increases with decreasing Pt:Au surface ratio, i.e. with reaching finer distribution of Pt atoms on the nanoparticle surfaces. Increasing reaction rate was associated with reducing surface coverage by CO_{ads}. No sign of poisoning by CO_{ads} was observed for the catalyst with the lowest Pt:Au surface ratio.

Chronoamperometic test showed that high activity of the catalyst with the lowest Pt:Au surface ratio is also associated with a high poisoning rate. It was postulated that too strong adsorption of a reactive or non-reactive intermediate other than CO_{ads}, or CO_{ads} formed as a product of CO_2 reduction by adsorbed hydrogen, are responsible for the deactivation of that catalyst.

The present study points out that high Pt dispersion on Pt–Au nanocatalyst, which is necessary for promotion of the dehydrogenation path in HCOOH oxidation, can produce too strong adsorption of poisoning species, because of high degree of electronic modification of Pt by Au. Therefore, in designing a Pt–Au nanocatalyst for HCOOH oxidation the Pt:Au ratio and the structure of the nanoparticles should be optimized with respect to a high selectivity toward dehydrogenation path and a low deactivation rate.

References

[1] X. Wang, J-M. Hu, I-M. Hsing, J. Electroanal. Chem. 562 (2004) 73–80.

[2] J. Willsau, J. Heitbaum, Electrochim. Acta 31 (1986) 943–948.
[3] A. Capon, R. Parsons, J. Electroanal. Chem. 44 (1973) 1–7.
[4] P.K. Babu, H.S. Kim, J.H. Chung, E. Oldfield, A. Wieckowski, J. Phys. Chem. B 108 (2004) 20228–20232.
[5] J. Solla-Gullon, V. Montiel, A. Aldaz, J. Clavilier, Electrochem. Commun. 4 (2002) 716–721.
[6] A. Cuesta, M. Escudero, B. Lanova, H. Baltruschat, Langmuir 25 (2009) 6500–6507.
[7] E. Rach, J. Heitbaum, Electrochim. Acta 32 (1987) 1173–1180.
[8] I.-S. Park, K.-S. Lee, J.-H. Choi, H.-Y. Park, Y.-E. Sung, J. Phys. Chem. C 111 (2007) 19126–19133.
[9] N. Kristian, Y. Yan, X. Wang, Chem. Commun. (2008) 353–355.
[10] N. Kristian, Y. Yu, P. Gunawan, R. Xu, W. Deng, X. Liu, X. Wang, Electrochim. Acta 54 (2009) 4916–4924.
[11] Y. Yu, Y. Hu, X. Liu, W. Deng, X. Wang, Electrochim. Acta 54 (2009) 3092–3097.
[12] X. Ge, X. Yan, R. Wang, F. Tian, Y. Ding, J. Phys. Chem. C 113 (2009) 7379–7384.
[13] M.D. Obradović, A.V. Tripković, S.Lj. Gojković, Electrochim. Acta 55 (2009) 204–209.
[14] M. Min, C. Kim, H. Lee, J. Mol. Catal. A: Chem. 333 (2010) 6–10.
[15] S. Kim, C. Jung, J. Kim, C.K. Rhee, S.-M. Choi, T-H. Lim, Langmuir 26 (2010) 4497–4505.
[16] Y.-C. Bai, W.-D. Zhang, C.-H. Chen, J.-Q. Zhang, J. Alloys Compd. 509 (2011) 1029–1034.
[17] A.V. Tripković, K.Dj. Popović, R.M. Stevanović, R. Socha, A. Kowal, Electrochem. Commun. 8 (2006) 1492–1498.
[18] L.R. Alden, D.K. Han, F. Matsumoto, H.D. Abruña, F.J. DiSalvo, Chem. Mater. 18 (2006) 5591–5596.
[19] W.X. Chen, J.Y. Lee, Z. Liu, Chem. Commun. (2002) 2588–2589.
[20] X. Li, W.X. Chen, J. Zhao, W. Xing, Z.D. Xu, Carbon 43 (2005) 2168–2174.
[21] L. Lu, G. Sun, H. Zhang, H. Wang, S. Xi, J. Hu, Z. Tian, R. Chen, J. Mater. Chem. 14 (2004) 1005–1009.
[22] A. Hugon, N.E. Kolli, C. Louis, J. Catal. 274 (2010) 239–250.
[23] I. Esparbé, E. Brillas, F. Centellas, J.A. Garrido, R.M. Rodríguez, C. Arias, P.-L. Cabot, J. Power Sources 190 (2009) 201–209.
[24] C.K. Poh, S.H. Lim, H. Pan, J. Lin, J.Y. Lee, J. Power Sources 176 (2008) 70–75.
[25] T.J. Schmidt, H.A. Gasteiger, R.J. Behm, Electrochem. Commun. 1 (1999) 1–4.
[26] A.A. Michri, A.G. Pshchenichnikov, R.Kh. Burshtein, Elektrokhimiya 8 (1972) 364.
[27] H. Angerstein-Kozlowska, B.E. Conway, A. Hamelin, L. Stoicoviciu, Electrochim. Acta 31 (1986) 1051–1061.
[28] E. Irissou, F. Laplante, S. Garbarino, M. Chaker, D. Guay, J. Phys. Chem. C 114 (2010) 2192–2199.
[29] M. Zhu, G. Sun, Q. Xin, Electrochim. Acta 54 (2009) 1511–1518.
[30] A. Rincón, M.C. Pérez, C. Gutiérrez, Electrochim. Acta 55 (2010) 3152–3156.
[31] J. Perez, A.A. Tanaka, E.R. Gonzales, E.A. Ticianelli, J. Electrochem. Soc. 141 (1994) 431–436.
[32] S. Kumar, S. Zou, Langmuir 23 (2007) 7365–7371.
[33] J.R. Kitchin, J.K. Nørskov, M.A. Barteau, J.G. Chen, Phys. Rev. Lett. 93 (2004), 156801-1–156801-4.
[34] J.R. Kitchin, J.K. Nørskov, M.A. Barteau, J.G. Chen, J. Chem. Phys. 120 (2004) 10240–10246.
[35] N.P. Lebedeva, M.T.M. Koper, E. Herrero, J.M. Feliu, R.A. van Santen, J. Electroanal. Chem. 487 (2000) 37–44.
[36] J. Kim, C. Jung, C.K. Rhee, T. Lim, Langmuir 23 (2007) 10831–10836.
[37] J.D. Lović, A.V. Tripković, S.Lj. Gojković, K.Dj. Popović, D.V. Tripković, P. Olszewski, A. Kowal, J. Electroanal. Chem. 581 (2005) 294–302.
[38] V. Grozovski, J. Solla-Gullón, V. Climent, E. Herrero, J.M. Felui, J. Phys. Chem. C 114 (2010) 13802–13812.
[39] F.J.E. Scheijen, G.L. Beltramo, S. Hoeppener, T.H.M. Housmans, M.T.M. Koper, J. Solid State Electrochem. 12 (2008) 483–495.
[40] J. Jiang, A. Kucernak, J. Electroanal. Chem. 520 (2002) 64–70.
[41] T. Smolinka, M. Heinen, Y.X. Chen, Z. Jusys, W. Lehnert, R.J. Behm, Electrochim. Acta 50 (2005) 5189–5199.
[42] N.P. Lebedeva, V. Rosca, G.J.M. Janssen, Electrochim. Acta 55 (2010) 7659–7668.
[43] G.L. Beltramo, T.E. Shubina, M.T.M. Koper, Chem. Phys. Chem. 6 (2005) 2597–2606.
[44] G.-Q. Lu, A. Crow, A. Wieckowski, J. Phys. Chem. B 103 (1999) 9700–9711.
[45] Y.X. Chen, A. Miki, S. Ye, H. Sakai, M. Osawa, J. Am. Chem. Soc. 125 (2003) 3680–3681.
[46] M. Osawa, K.-I. Komatsu, G. Samjeske, T. Uchida, T. Ikeshoji, A. Cuesta, C. Gutierrez, Angew. Chem. 50 (2011) 1159–1163.
[47] Y.-X. Chen, M. Heinen, Z. Jusys, R.J. Behm, Chem. Phys. Chem. 8 (2007) 380–385.